Multi-responsive 3D printable organohydrogel for the fabrication of durable and low-hysteresis flexible sensors

Applied Materials Today 44 (2025) 102675

Contents lists available at ScienceDirect

Applied Materials Today

journal homepage: www.elsevier.com/locate/apmt

Multi-responsive 3D printable organohydrogel for the fabrication of durable and low-hysteresis flexible sensors

Giorgio Mogli [a], Ignazio Roppolo [a], Annalisa Chiappone [b], Stefano Stassi [a,*]

[a] Department of Applied Science and Technology, Politecnico di Torino, C.so Duca degli Abruzzi 24, 10129 Turin, Italy
[b] Dipartimento di Scienze Chimiche e Geologiche, Università degli studi di Cagliari, Cittadella Universitaria Blocco D, S.S. 554 bivio per Sestu 09042 Monserrato, CA, Italy

ARTICLE INFO

Keywords:
Organohydrogel
Wearable sensors
3D printing
Glycerol
Temperature sensing

ABSTRACT

Ionically conductive hydrogels have emerged as promising candidates for sensors in wearables and prosthetics due to their high flexibility and stretchability. However, those suffers intrinsically of a strong limitation which is water evaporation, that over time alters their mechanical and electrical properties, restricting their usage. On the other hand, the use of organohydrogels limits this drawback, controlling rate of evaporation and thus preserving the device properties. This study introduces a double-network, conductive, 3D-printable hydrogel where water is partially replaced by glycerol using a solvent replacement strategy to prevent evaporation and preserve electrical and sensing properties. This organohydrogel exhibits excellent stretchability (up to 350 %), high strain and pressure sensitivity, and negligible hysteresis. Moreover, the mechanical and electrical characteristics of the organohydrogel remain stable for more than six months. The sensor demonstrates an outstanding strain detection limit of 0.05 % and a pressure detection limit of 1.5 Pa, enabling the evaluation of micrometric deformations across a wide temperature range, including below room temperature. The use of glycerol, a high boiling point and biocompatible solvent, allows both temperature and humidity sensing, enhancing the versatility of this organohydrogel. Since the solvent replacement strategy is applied to the already formed hydrogel, its 3D printability remains unaffected, enabling the enhancement of sensing properties through complex 3D structuring. The excellent time stability of mechanical and sensing properties, combined with sensitivity to both micro and macro deformations, temperature and humidity responsiveness, highlights the potential of this organohydrogel in a broad spectrum of flexible sensing applications.

1. Introduction

In the last years, the advancement in IoT, brain computer interfaces and smart electronic devices have brought to attention the need of an effective link between the electronic and the human worlds [1,2]. While the machine world is characterized by rigid elements, living matter is distinguished by soft and flexible tissues. Therefore, flexible electrically conductive materials could improve the human interactions with the machines by substituting traditional metal or semiconductor devices [3,4]. In flexible sensors field, piezoresistivity [5–7], piezocapacitance [8–10], piezoelectricity [11,12] and triboelectricity [13–15] are commonly exploited to transduce the external stimuli into an electrical parameter that can be elaborated and transmitted, fundamental tasks in an IoT based world. Moreover, in the last year 3D printing technology has been increasingly employed in flexible sensors fabrication [16–18] since it ensures reproducible devices with elaborated geometry that can significantly enhance sensors performances and facilitate their application [16,19,20]. Human-health continuous monitoring [21,22], soft-robotics [23,24], brain computer interfaces [25,26] and every other field in which a human-machine interaction is needed, may benefit from flexible sensors applications.

In this scenario, hydrogels, polymeric networks that retain a great amount of water, represent a possible solution due to their easily adjustable mechanical properties and intrinsic softness [27–29]. In addition, hydrogels can be provided by electrical conductivity thanks to the dissolution of conductive metallic or carbonaceous fillers [30–32], employing conductive polymers [33,34] or exploiting ions mobility through their water-rich environment [35,36], making them usable in sensors field.

Hence, electrically conductive hydrogels are proper choice to

* Corresponding author.
E-mail address: stefano.stassi@polito.it (S. Stassi).

https://doi.org/10.1016/j.apmt.2025.102675
Received 29 December 2024; Received in revised form 14 February 2025; Accepted 6 March 2025
Available online 13 March 2025

develop the so-called flexible or smart sensors that can be responsive to different external stimuli, such as deformations, temperature and humidity [37–39], including 3D printable ones [40,41].

Nevertheless, water evaporation is a well-known issue related to the hydrogels' employment in sensors [42,43]. This problem leads to a long-time instability in electrical and mechanical properties, limiting their large-scale application in every-day life. Several strategies have been investigated to overcome this issue, such as encapsulating surfaces of hydrogel with impermeable layers [44,45] or substituting the water with high boiling point organic solvents, like glycerol and ethylene glycol [46–48]. Considering the latter, the literature presents various approach to partially substitute the water, in order to obtain organohydrogels with anti-freezing and anti-drying properties thanks to the higher density of hydrogen bonds between water and organic solvent molecules [49–51]. The direct polymerization in a binary solvent composed of water and an organic solvent [52,53] or the infusion of the same binary solvent into the dried hydrogels [54] are potential ways to achieve organohydrogels. However, the first strategy could influence the solubility of precursor monomers and hinder the polymerization process [55]. While the second strategy involves two-steps, dehydration of hydrogel and then the infusion of the organic solvent, which not always easily enter into the dried polymeric network. Another investigated strategy consists in replacing the inner water of hydrogels by immersion into organic or binary water-organic solvent [56–58]. The so-called "solvent replacement strategy" represents an universal strategy since some hydrogels' features, like preparation process and 3D printability are kept unchanged since the polymerization process still happens in water medium [59].

Recently we developed hydrogel sensor, based on a poly(vinyl alchool)-acrylic acid double network, crosslinked by poly(ethylene glycol diacrylate) [60]. Based on those findings, here we investigate solvent replacement strategy with a binary water-glycerol solvent to address water-evaporation issues of the already studied hydrogel. The resulting organohydrogel, maintained an optimal stretchability (up to 350 %) and flexibility, good sensitivity to external tensile and compressive stimuli and showed an exceptional both mechanical and electrical stability over 6 months of testing. The effect of glycerol helped to obtain lower-hysteresis samples, with much repeatable electrical response with respect of starting hydrogel. Moreover, adopting solvent replacement on the already made hydrogel, its 3D printability is not affected, and it is still possible to exploit the enhancement of sensing properties given by 3D complex structuration. Outstanding strain (0.05 %) and pressure (1.5 Pa) limit of detection were found and the capability to sense both slow and quick deformations was proven. In addition, the presence of glycerol provides the material with wide temperature range stability and atmospheric water retention, enabling sensitivity to both temperature and humidity. The versatility of the presented sensors under different deformation stimuli and various environmental conditions demonstrates the applicability of the ionically conductive poly (vinyl alcohol)-poly(acrylic acid) organohydrogel across several disciplines, ranging from soft robotics to wearables.

2. Materials and methods

Poly(vinyl alcohol) (MW 89 000–98 000 Da, 99 + % hydrolyzed, PVA), acrylic acid (AAc), poly (ethylene glycol diacrylate) (average MW 575, PEGDA575), water-soluble diphenyl(2,4,6-trimethylbenzoyl) phospine oxide-based nanoparticle photoinitiator containing ionic surfactant (TPO-SDS), tartrazine, sodium chloride (NaCl) and glycerol were purchased from Sigma Aldrich (USA).

2.1. PVA/AAc/NaCl organohydrogel sensors preparation

The UV-reactive formulation was prepared and light cured or 3D printed following the same procedure presented in our previous works [60,61]. Afterwards, dumbbell-shaped samples for the tensile tests were produced by casting the ink and irradiating it under nitrogen flux, to avoid oxygen inhibition of photopolymerization reaction. A UV lamp (Hamamatsu LC8) was applied with a power density of 20 mW cm^{-2} for 4 mins. Dumbbell-shaped samples with 30 mm length, 12 mm gauge length, 9 mm width, 3 mm gauge width, and 3 mm thickness were tested. A commercial DLP printer (Asiga MAX X UV385) with light emission wavelength centered at 385 nm and nominal resolution of 27 × 27 μm^2 was employed to fabricate 3D samples. This equipment was coupled with a vaporizer (TaoTronics TT-AH002, vapor flux 30 mL h^{-1}) to mitigate water evaporation during 3D printing process. The printing parameters of the hydrogel were explored in our previous works [29, 60]. Stainless steel electrodes were placed after the printing/casting process and were glued employing the same liquid formulation, which was then polymerized on the specimens by performing 5 mins irradiation in a UV chamber (Robofactory). A binary solution of deionized water and glycerol (1:4 wt ratio) with 1 M of sodium chloride (NaCl) was prepared for solvent replacement strategy. PVA/AAc/NaCl organohydrogel samples were prepared by immersing PVA/AAc/NaCl hydrogel samples into 25 mL of binary solution for different times.

2.2. Physicochemical analysis

TGA was performed using a thermogravimetric analyzer NETZSCH TG 209 F3 Tarsus (Selb, Germany). Weight decrease related to thermal degradation was followed between 30 and 800 °C (heating rate 10 °C min^{-1}), employing a standard air atmosphere (airflow 20 mL min^{-1}), with N_2 as a protective gas (flow 20 mL min^{-1}). Evolving gases were then directly directed to FT-IR spectrophotometer and analyzed. The spectra were acquired by averaging 64 scans (64 for the background spectrum too) in 4000–600 cm^{-1} range with a resolution of 2 cm^{-1}. To better visualize the data, IR spectra were normalized with respect to the maximum peak in the O—H stretching area located at around 3600 cm^{-1}. Those measurements were carried out using a Bruker Tensor II Fourier transform spectrophotometer (Billerica, MA, USA) directly connected to TGA instrument by a transfer line. Spectra were scaled to a 0–1 range to improve qualitative visualization.

2.3. Electromechanical characterizations

Tensile and compressive tests were performed through a universal testing machine (FZ3-X500, Test Engineering) coupled with a load cell of 500N. Sensors' electrical performances were evaluated by means of a LCR meter (BK 894, B&K Precision). A parallel between a resistor (R_p) and a capacitor (C_p) was used to model the sample impedance. For all the electrical measures a voltage amplitude of 500 mV and a testing frequency of 1000 Hz were set and piezoresistive behaviour was considered. Single tensile tests were conducted on dumbbell-shaped samples at velocity of 10 mm min^{-1}, while cyclic tensile trials were performed at 20 mm min^{-1} fixing the maximum deformation at 50 % and repeating 50 cycles of stretching-releasing. Compressive tests of the 3D printed structures were conducted using a velocity of 1 mm min^{-1}. A pre-load of 50 mN was set to compensate slight imperfection of the flat upper surface of samples. Copper sheets were used as electrodes. Cyclic compressive tests of 25 subsequent cycles were carried out using the same setup.

Compression static trials were performed by applying small weights (20, 70, 170, 370, and 870 mg) on the top surface of printed sensors. Weights were applied on a laboratory glass, in which the upper copper electrode was attached to. This structure, that weighed 1.5 g, served to distribute the load to the whole upper surface of the samples.

Humidity sensitivity was tested by placing organohydrogel samples in a climatic chamber (KeyKratos™ Plus 01.05.XX). Temperature was fixed at 25 °C and relative humidity (RH) was increased from 30 % to 95 % with step of 10 %. Resistance and capacitance of sensors were acquired for each RH step through 1-minute-long acquisition once the chamber humidity was stable. The average values over the acquisition

time were then considered.

Conductivity of samples was measured by placing them between two parallel copper electrodes and measuring an average R_p over 1 min acquisition. Conductivity was then computed using the formula:

$$\sigma = \frac{d}{R_p A}$$

where d is the distance between the two electrodes, R_p is the parallel resistance and A is the surface area of the samples.

Relative resistance variations ($\Delta R/R_0$) and relative capacitance variations ($\Delta C/C_0$) were computed according to the following formula:

$$\frac{\Delta X}{X_0} = \frac{X(t) - X_0}{X_0}$$

where X is the parallel resistance or capacitance measured at a certain time t and X_0 is its value when no load is applied.

Sensitivity (S) or Gauge Factor (GF) for piezoresistive transduction mode was evaluated using:

$$S = \frac{\frac{\Delta R}{R_0}}{\varepsilon}$$

where ε is the tensile or compressive deformation applied to the sample.

2.4. Dynamic mechanical thermal analysis (DMTA)

DMTA experiments were carried out using a Triton Technology-TTDMA, the dynamic-mechanical testing was coupled with impedance measurement. Samples of $1.20 \times 5 \times 10.5$ mm^3 were tested. Electrical (R_p) and mechanical (Young's modulus) properties dependency from temperature was evaluated in a temperature range from 0 °C to 80 °C using a heating rate of 3 °C min^{-1}. During the test, the specimens were subjected to a fixed cyclic deformation (200 μm) with a constant frequency of 1 Hz. Small deformation piezoresistive test was evaluated performing DMTA analysis at decreasing displacements (200 μm, 100 μm, 50 μm, 10 μm, 5 μm, 2.5 μm) at RT. Displacement frequency was varied from 0.1 Hz to 2 Hz, to assess how sensing performance is affected by the load application frequency. In both the experiments, two conductive wires were clamped with the sample edges at the DMTA grips. The conductive elements were electrically isolated from the metallic parts of the instrument through polyimide foils.

2.5. Differential scanning calorimetry (DSC)

DSC measurements were performed with a Netzsch DSC 204 F1 Phoenix instrument, equipped with a low temperature probe. All the tests were performed in nitrogen atmosphere with the following thermal method: 5 min isotherm at – 40 °C, heating ramp between −40 °C and 80 °C with a heating rate of 10 °C min^{-1}, 5 mins isotherm at 80 °C, cooling cycle 80 °C-40 °C with a cooling rate of 10 °C min^{-1}, and then cycle is repeated. The reported curves are relative to the second heating/cooling steps.

3. Results

The organohydrogel was developed starting from an already studied ionically conductive 3D printable polyvinyl(alcohol) (PVA)/acrylic acid (AAc)/ sodium chloride (NaCl) hydrogel, aiming at improving its stability by preventing water evaporation, which constitute the main limitation in hydrogel sensing applications [60]. The starting hydrogel is constituted by a semi-interpenetrated network, based on a chemical covalent network of AAc, crosslinked by PEGDA, that entraps physical network made by PVA, The hydrogel is endowed with ionic conduction by dissolving sodium chloride (NaCl) salts in the precursor water. Acrylic Acid and PEGDA, in the presence of a water-soluble photoinitiator (TPO-SDS) can react through a light-induced radical polymerization forming a chemically crosslinked network. This assures the 3D printability of the hydrogel through Digital Light Processing (DLP) with good resolution and sufficient mechanical stability. Highly flexible PVA chains that are physically entrapped in the covalent network improve the ion mobility as discussed in our previous research [60]. Tartrazine was also added to the formulation as water-soluble dye aiming to improve the x-y resolution of the printed hydrogel limiting the light diffusion in the printing vat. Briefly, hydrogel weight percentages are roughly 63.68 % of NaCl water solution (1 M), 15.92 % of PVA, 19.90 % of AAc, 0.20 % of PEGDA575, 0.30 % of TPO-SDS and 0.006 % of tartrazine (Fig. 1a, Table S1a). It was already demonstrated that the hydrogel shows good electrical, mechanical and sensing properties, however both conductivity and elastic modulus are poorly stable if stored at room temperature conditions and not in a humid environment [60]. In order to overcome this hydrogel's application limitation, a solvent replacement strategy was here adopted. Glycerol was chosen as organic solvent having high boiling point and, in view of wearable applications, because not toxic or harmful. To maintain mobile ions (Na^+ and Cl^-) inside the samples, it was necessary to avoid an excessive osmotic pressure towards the solvent by dissolving NaCl into the organic solvent too; therefore, taking into account the limited NaCl solubility in pure glycerol [62],a binary organic solvent composed by 4 parts of glycerol and 1 part of deionized water was prepared (Gly:DIW). This choice could effectively improve the long-term mechanical and electrical stability of the material thanks to the high density of hydroxyl groups in glycerol that results in the formation of hydrogen bonds with water free molecules, hindering the water crystallization, and with the polymeric network itself increasing the intermolecular interactions among PVA and PAA chains [63,64]. Then, 1 M of NaCl was dissolved into the binary solution by stirring at 40 °C. The 3D printed or photocured PVA/AAc/NaCl samples were immersed in this solution for different times to allow the binary solvent to enter within the polymeric network, substituting the hydrogel water. This process resulted into the PVA/AAc/NaCl organohydrogel formation. The hydrogel structure and the organohydrogel preparation are summarized in Fig. 1a.

Weight analysis was the first essay used to evaluate the binary solvent presence in the hydrogel, investigating different immersion times. In Fig. 1b the weight changes of PVA/AAc/NaCl samples immersed in Gly:DIW 1 M NaCl solution at different hours of immersion are reported. Samples weight diminished in the first hours of immersion, reaching a maximum decrease of 40 % after 2 h. This can be related to a water/glycerol exchange, with water that apparently exits from the matrix more rapidly than how glycerol enters. Then, it was measured a subsequent increase of weight, and after 5 days of immersion the weight of samples recovers almost the initial weight, remaining stable and evidencing that equilibrium was reached.

To support these assumptions, thermogravimetric analysis (TGA) coupled with infrared spectroscopy of evolved gases were carried out on the samples immersed for different time steps. Time points of 2 h (*2h*), 5 days (*5d*) were analysed, since those correspond to the maximum weight variation and the initial equilibrium state respectively. Samples immersed for 10 days (*10d*) were also considered, to investigate possible changes of PVA/AAc/NaCl organohydrogels after equilibrium condition is reached. The organohydrogels investigated in this work are summarized in Table S1b.

Observing thermogravimetric analyses and their first derivatives (figure S1), hydrogel sample shows a consistent weight loss around 100 °C (figure S1a), which is related to the water loss. The first derivative peak associated to water evaporation is less prominent in the organohydrogels. Conversely, the organohydrogels evidence a weight loss at higher temperature, which can be related to the presence of glycerol. In fact, glycerol starts its degradation at about 180 °C (figure S1b), reaching its maximum rate of degradation (DTG peak) at around 250 °C. The glycerol first derivative peak is evident in 2 h organohydrogel (figure S1c), indicating that glycerol entered the *2 h* sample too, and

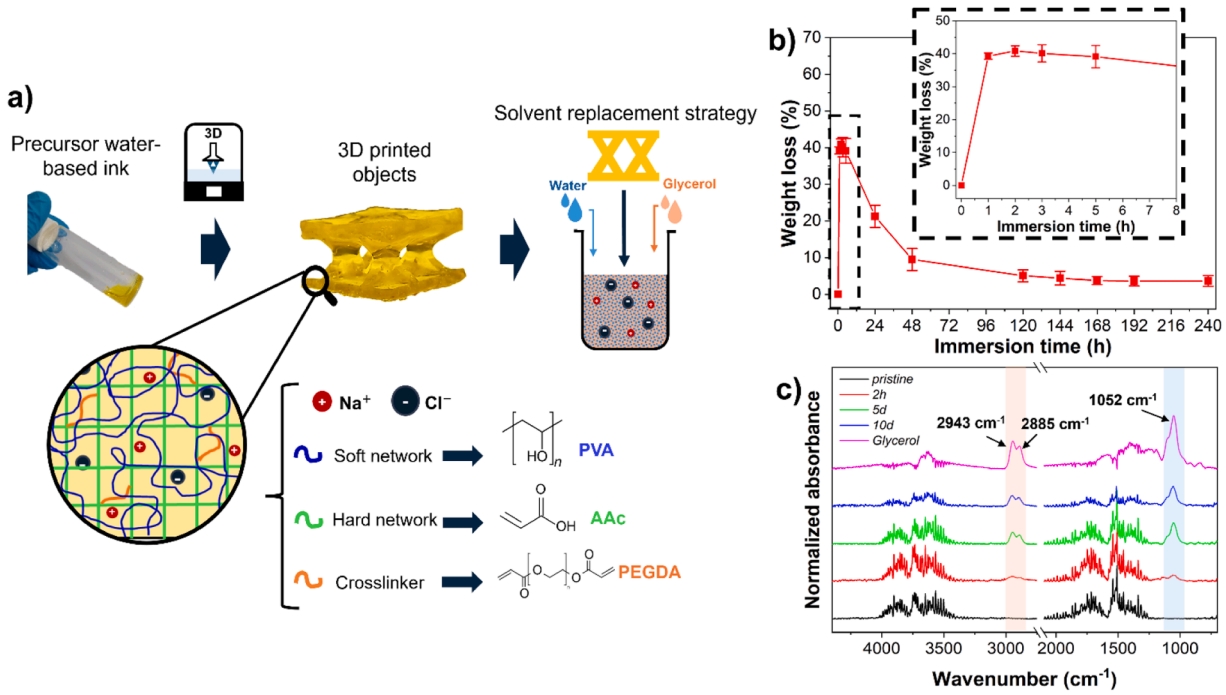

Fig. 1. (a) PVA/AAc/NaCl organohydrogel preparation through the solvent replacement method. At the bottom, the composition of the precursor hydrogel. (b) Weight loss of 5 independent organohydrogel samples after immersion into the binary Gly:DIW solvent for different time steps. In the inset, the magnification of the first hours of immersion. (c) IR spectra of evolved gas at 180 °C resulting from the thermogravimetric analysis.

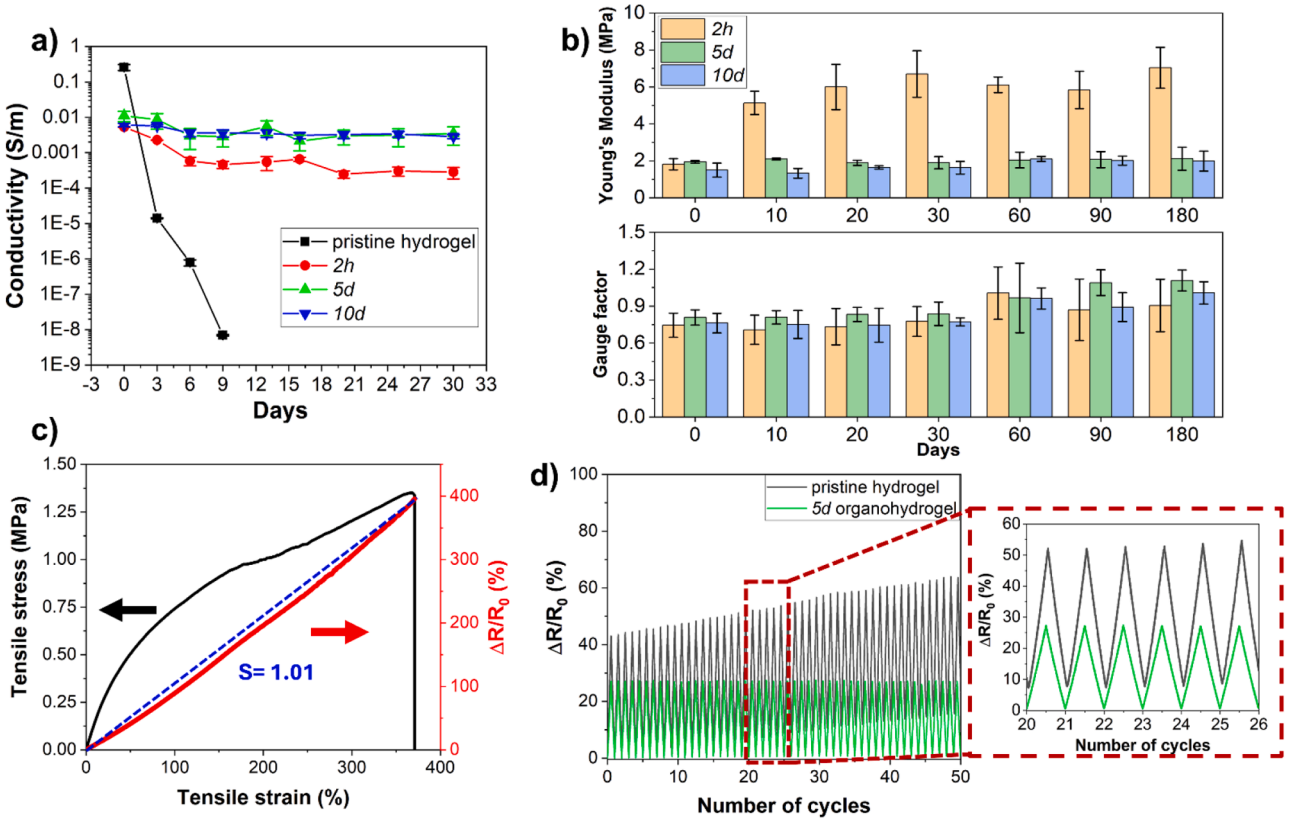

Fig. 2. (a) Electrical conductivity of hydrogel and organohydrogels samples over 30 days of testing. The pristine hydrogel measures were interrupted after 9 days due to the high resistance of the samples in a plate-plate configuration. Five independent samples were tested. (b) Young's modulus (up) and gauge factor (down) of organohydrogel samples subjected to tensile test up to 50 % of strain for 180 days. Five independent dumbbell-shaped samples were tested for each typology. (c) Tensile strain-stress curve of a 5d organohydrogel sample in black. Piezoresistive characteristic curve of a 5d organohydrogel sample in red. Blue dashed line highlights the linear fitting (R^2=0.998). Sensitivity value (S) is reported in blue. (d) Resistance variations of hydrogel and 5d organohydrogel samples subjected to cyclic tensile test up to 50 % of strain for 50 successive cycles. On the right a magnification of few cycles is reported.

obviously even in the samples with longer immersion time (figure S1d-e). These hypotheses were confirmed analysing IR spectra (Fig. 1c) at flash point of glycerol (180 °C), namely the initial temperature in which vapour is formed. Samples immersed 5 and 10 days clearly show the peaks associated with C—H asymmetric stretching at 2885 cm^{-1} and 2943 cm^{-1} and the peak located around 1052 cm^{-1}, related to C—O bond stretching. These peaks can be uniquely related to glycerol, since the temperature at which IR are analysed is lower than the onset of polymer degradation (figure S1f), that starts at around 250 °C. In *2 h* sample, this IR peak and the one located at around 1052 cm^{-1} are slightly visible but confirm glycerol presence.

While we can assume that in the neat hydrogel the ion movements mainly take place in the liquid water phase that is just supported by the soft polymeric network, the presence of glycerol increases the viscosity of the binary solvent with respect to pure water and creates a more rigid polymeric network through the formation of intermolecular hydrogen bonds as reported in figures S2a and S3a. Therefore, a greater viscosity of the transport medium and a higher rigidity of the polymer network, result in lower ions mobility [65,66] and therefore to a decrease of electrical conductivity in organohydrogels with respect to the pristine hydrogel, as shown in figure S2b. Moreover, since the conductivity is provided by free ions in the liquid phase, the lower content of transport medium, as observed by weight analysis for *2 h* samples, leads to a lower ionic species content and, consequently, to an overall lower conductivity among the organohydrogels.

Nevertheless, organohydrogels showed significantly higher stability of electrical conductivity over time if stored at room temperature in air condition. While the pristine samples conductivity diminished of 8 orders of magnitude after only 9 days of testing, the *2 h, 5d, 10d* organohydrogels showed lower variations of electrical conductivity over a month of testing (Fig. 2a). In particular, samples immersed 5 and 10 days owned more stable conductivity than *2 h* samples, which displayed a reduction of about 1 order of magnitude after 1 month.

Electromechanical tensile tests were performed on dumbbell shaped samples to evaluate mechanical and electrical response to strain deformations. All the kinds of PVA/AAc/NaCl organohydrogels owned excellent tensile properties. They all exhibited ultimate tensile strain higher than 300 % (figure S2b) in line with other organohydrogels present in literature [67–70]. Solvent-replacement strategy brought to an enhancement of the samples' stiffness, in fact Young's modulus increased by almost 6 times after two hours of solvent replacement compared to the pristine hydrogels' samples, as shown in figure S3a. This is due to glycerol that may hinders chains movements causing increase of elastic modulus.

Tensile tests were coupled with electrical measures, in order to investigate the piezoresistive response of the sensors to external deformation stimuli. Resistance variations with respect to the initial resistance at no strain conditions, were monitored for each sample. All the organohydrogel samples showed a positive piezoresistive response, with a strain sensitivity (or gauge factor) in the first linear range, comprised between 0 % and 50 % of strain, slightly lower than PVA/AAc/NaCl hydrogel (figure S3b).

Electromechanical tensile tests were performed on the same samples over a long time period (6 months), to investigate the durability of *2 h, 5d, 10d* PVA/AAc/NaCl organohydrogels. Sensors were deformed until 50 % of tensile strain and, since resistance variation in this range is almost linear (fig S4a), sensitivity was computed. In Fig. 2b (top) Young's moduli of the three organohydrogels investigated, are reported. Stiffness of *2 h* samples almost doubled after 10 days. Then it remained quite stable in the subsequent days of measures. Apparently, the binary water-organic solvent at 2 h of immersion is not effectively diffused into the polymeric matrix. Therefore, the small amount of inner water left inside the hydrogel evaporates after few days, leading to an increase of Young's modulus. Instead, at both equilibrium conditions, namely *5d* and *10d* samples, there are no remarkable variations of Young's modulus after 180 days of testing, sign that solvent replacement strategy is effective. Piezoresistive gauge factors in 0 %−50 % strains range, namely the sensitivity, was around 0.85 for all the kinds of organohydrogel. 0 %−50 % strain was the investigated range since it corresponds to the standard value related to human motion [71]. It remained almost stable over the measurement period except for a slight growth noticed after the first month (Fig. 2b, bottom). *5d* samples were further characterized, considering that five days is the minimum time of immersion to reach equilibrium conditions and stable mechanical and electrical properties.

Those organohydrogels samples were able to be stretched >350 % of strain before rupture and owned a positive piezoresistive transfer curve, since the more the sample is stretched, the longer is the path between electrodes that ions must traverse [72]. The overall curve is well approximated by a linear model with a gauge factor of 1.01 (Fig. 2c).

Repeatability of material response was assessed through electromechanical cyclic tensile test. Mechanical hysteresis resulted lower with respect to the pristine hydrogel, as shown in figure S4b. Therefore, glycerol presence helps to reduce the viscous response of the polymeric network. This is reflected by the electrical response of PVA/AAc/NaCl organohydrogel. In 50 consecutive cycles at 50 % of strain the *5d* organohydrogel presents a much lower resistance drift than pristine hydrogel, sign that the resistance at no strain applied is repeatable among the cycles of deformation (Fig. 2d). Moreover, the cycles amplitude remains stable over the cycles.

Since it was demonstrated that glycerol effectively enhanced sensor mechanical and electrical stability over time, the organohydrogel behaviour in a wide temperature range, that could reflect the conditions in a potential every-day application, was investigated. Dynamic mechanical thermal analysis (DMTA) was used to assess the temperature dependency of the *5d* organohydrogel mechanical properties. Since, samples were deformed cyclically through DMTA analysis, electrical resistance was measured by inserting two cables in the clamping system to investigate the electrical response too (Fig. 3a). The test was performed from 0 °C to 80 °C. At sub-zero temperatures the electrical signal was very noisy (figure S5a), making it impossible to characterize the sensor response to small deformations, although cyclic variations in resistance could still be seen (figure S5b). Nevertheless, it is worth to mention that the organohydrogel possesses anti-freezing properties, as witnessed by the DSC thermograms reported in figure S6. For what regards DMTA, within the investigated range, E' value are below 2 MPa, without showing drastic changes of value. This is consistent with specimens that at the tested temperatures are below glass transition temperature (T_g). Unfortunately, T_g cannot be measured due to solidification of the glycerol, which would make unfeasible this measurement. Nevertheless, it is worthy to recall that Young's modulus is expected to decrease with the increase of temperature, since thermal energy facilitates polymeric chains movements, weakening the hydrogens bonds between the binary solvent and the polymer [73,74]. Similarly, the ionic mobility increases, and thus conductivity increase [36]. The tests show that in the measurement range the Young's modulus decreases of about 50 % while the sample resistance decreases of two orders of magnitude (Fig. 3b).

Interestingly, resistance signal of the sample was able to follow the small cyclic deformation of 200 μm, corresponding to 1.87 % of tensile strain, applied to the sample during the test, as shown in the zoom reported in Fig. 3c. Therefore, the relative resistance amplitude of each cycle, called Δ, was computed as the percentual variation of the peak with respect to the previous valley (inset formula in Fig. 3c). This variable is a sign of the sensor sensitivity at a strain of 1.87 %, since the electrical resistance has a positive linear dependence on the strain, as previously shown in the 0–50 % range. The red line in Fig. 3b represents how the Δ value depends on the temperature. It is worth noting that sensitivity, namely the Δ values divided by the correspondent strains, decreases while temperature increases. Increased polymeric chains mobility and enhancement of ions vibrational energy play the main roles in this effect. The enhanced ions mobility at higher temperature is less

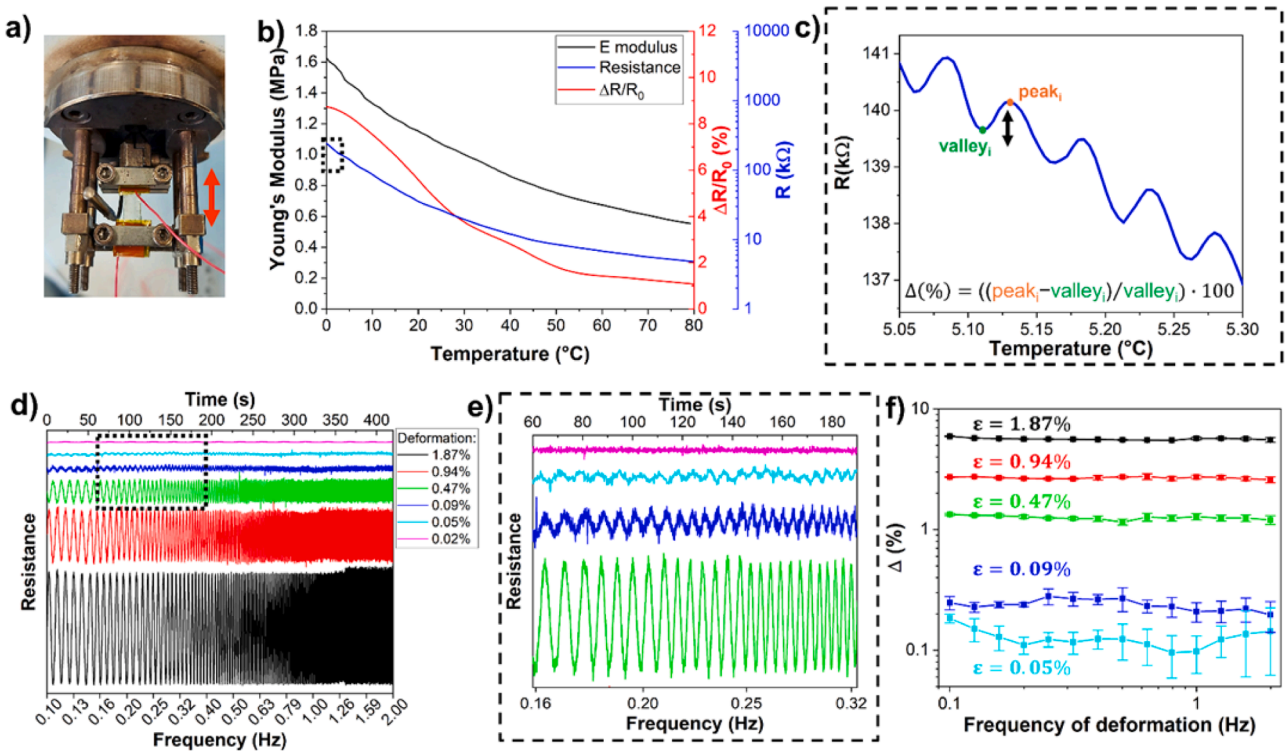

Fig. 3. (a) Image of the DMTA setup, coupled with electrical measures. (b) Young's modulus, electrical resistance and Δ dependency from temperature of a 5d sample subjected to DMTA analysis. (c) The enlargement of the area underlined by dashed rectangle in Fig. 4b. The resistance response of 5d sample underwent to cyclic deformations during DMTA analysis is reported. In the inset, the formula adopted to compute the amplitude of cycles (Δ). (d) Resistance curves of 5d sample subjected to different cyclic strains at frequencies comprised between 0.1 Hz and 2 Hz. The test was performed at room temperature. Deformations of 1.87 %, 0.94 %, 0.47 %, 0.09 %, 0.05 % and 0.02 % were considered. Response curves were vertically shifted for better clarity. (e) Enlargements of the area between 0.16 Hz and 0.32 at low strains. (f) Average Δ at the different frequencies for the strains considered (logarithmic scale). The standard deviations are referred to the variability of Δ in cycles at same frequency.

affected by external deformations, leading to smaller resistance variations. Therefore, as expected, sensitivity is affected from both deformation and temperature contributions. These results show that PVA/AAc/NaCl organohydrogel could be employed also as temperature sensor with a negative resistive thermal dependency.

Since DMTA allows the application of small tensile deformations, the *5d* organohydrogel was tested at very small tensile strains at fixed room temperature (25 °C) in order to investigate its limit of detection. In parallel, frequency of deformation was increased from 0.1 Hz to 2 Hz to explore if the sensor could follow rapid deformations from the electrical point of view. Each frequency of deformation was maintained for 30 s. The electrical response of the *5d* organohydrogel to different strains (1.87 %, 0.94 %, 0.47 %, 0.09 %, 0.05 % and 0.02 %) is reported in Fig. 3d. Considering the enlarged sections in the Fig. 3e, resistance variations are evident until 0.05 % of strain. The *5d* organohydrogel seems no more sensitive to 0.02 % of tensile strain due to the prevailing electrical noise. Therefore, the limit of strain detection resulted 0.05 %. As described before, the resistance variations between peaks and valleys (Δ) of each cycle were derived. Then, for each deformation frequency considered, average values and standard deviations of Δ were computed and reported in Fig. 3f. As can be seen, the amplitude of resistance cycles remains quite stable for all the strains in the frequency range considered although standard deviations slightly higher for 0.09 % and 0.05 % strains, due to the challenging identification of peaks for higher frequencies and the electrical noise impact. From this results it can be assumed that sensitivity of *5d* organohydrogel is independent from deformation frequencies among 0.1 Hz and 2 Hz.

Furthermore, PVA/AAc/NaCl organohydrogels exhibited a good responsiveness to environmental humidity variations. Indeed, the -OH rich structure of organohydrogel, given by glycerol presence, is able to absorb the water molecules from the atmosphere [75]. When external relative humidity increases, water molecules number within the polymeric network grows, facilitating ion migration by providing a less viscous transport medium. This is macroscopically reflected by a greater ionic current resulting in a decrease in electrical resistance as shown in the inset of Fig. 4a. On the other hand, organohydrogel sensors were able to monitor humidity changes through capacitance variations too. In fact, capacitance depends on sensors geometry and material permittivity as ideally described by the formula related to parallel plates capacitors:

$$C = \varepsilon_0 \varepsilon_r \frac{S}{d}$$

Where ε_0 is the vacuum permittivity $\left(8.854 \cdot 10^{-12} F/m\right)$, ε_r is the relative permittivity of the material between the plates and S and d are respectively the plates surface and the distance between them. In particular, relative permittivity of water is much higher than air one. Therefore, as water amount inside the sensor increases, capacitance rises due to the increase in relative permittivity. PVA/AAc/NaCl organohydrogel sensors were placed in a climatic chamber and relative humidity was varied from 30 % to 95 %, while temperature was kept constant at RT. Electrical resistance and capacitance were monitored for each humidity step considered. The resistance and capacitance responses referred to their values at 30 % RH are reported in Fig. 4a and 4b, respectively. While the resistance response is linear, with sensitivity of 1.27, capacitive sensing mode shows an exponential behaviour with larger relative variations of capacitance and thus greater sensitivity.

3D printing has been proven to represent an effective tool for obtaining complex structures that enhanced sensitivity of sensors [60]. Since solvent replacement strategy has been successful applied on polymerized hydrogels, this approach could be employed to prepared

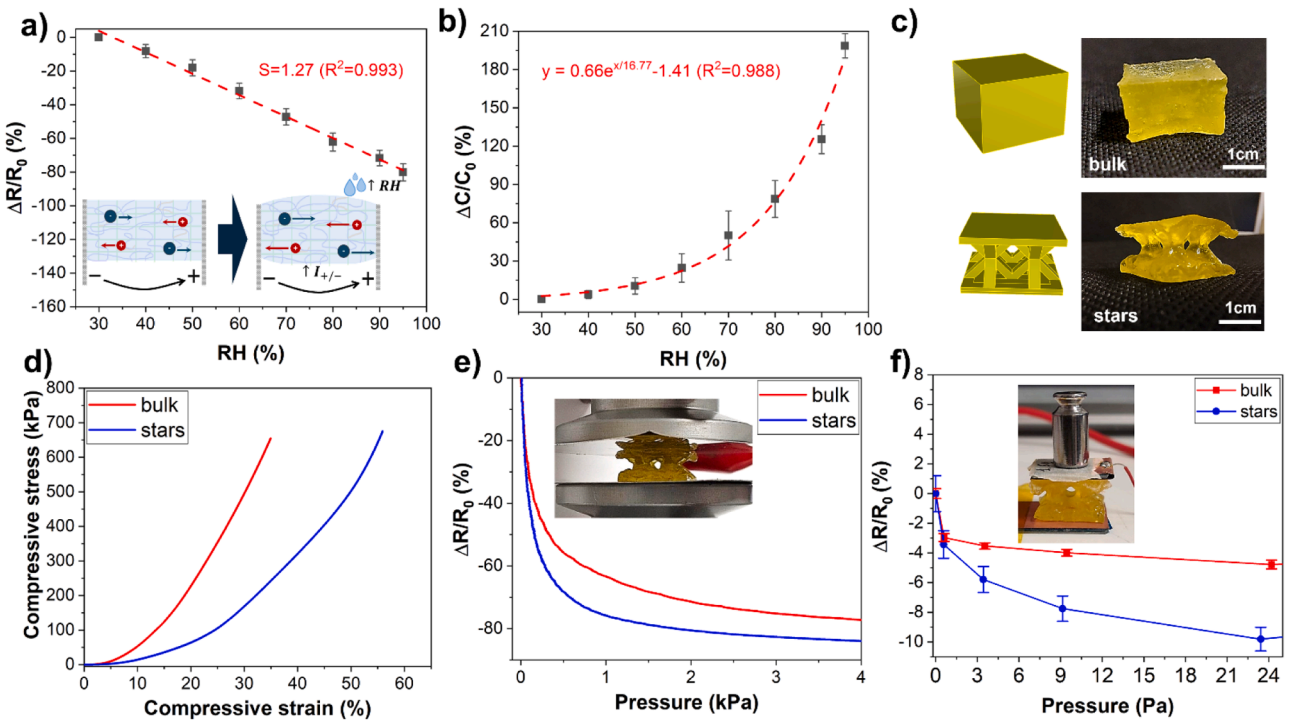

Fig. 4. . Organohydrogel electrical resistance (a) and capacitance (b) response under relative humidity changes. In the inset (a), the scheme of humidity sensing mechanism is reported. Five independent dumbbell-shaped samples were tested (c) Digital models (left) and their 3D printed organohydrogel versions (right). (d) Compressive stress-strain curves of 3D printed "bulk" and "stars" models. (e) Relative resistance variations during dynamic compressive trials of "bulk" and "stars" structure. In the inset, the setup for "stars" sample. (f) Relative resistance variations of bulk and stars 3D printed samples under the application of small static weights. In the inset, the setup for "stars" sample.

complex shape PVA/AAc/NaCl organohydrogel too. A Digital Light Processing (DLP) printer was employed to fabricate 3D models with the precursor photocurable PVA/AAc/NaCl ink, as explored in detail in our previous works [29,60]. "Bulk" and "stars" models were 3D printed and then immersed in the Gly:DIW solution (1M NaCl) for 5 days (Fig. 4c). Compression electromechanical tests were carried out to evaluate their performances as pressure sensors. As expected, 3D printed stars presented a lower stiffness and larger deformations at same pressures with respect to the bulk structure (Fig. 4d). Mechanical test was coupled with electrical measurement and electrical resistance was referred to the resistance of the samples with no load applied (Fig. 4e). Resistance diminished when load increased, due to the reduction of the path that ions must cross between the electrodes. Therefore, since "stars" structure is more deformable under the same load, the ions' path is further reduced, and resistance variations are more significant. The sensitivity of both structures reaches its maximum under 500 Pa, then diminishes at higher load. Consequently, electrical response to very small loads was investigated by applying small weights on the samples step-by-step. For each weight, the electrical resistance was measured for 1 min and then its averaged value and its standard deviation were considered (Fig. 4f). The two structures could detect a small pressure of 1.5 Pa, with a resistance variation slightly higher for "stars" sample, but in both cases, it was around 3 %. However, "stars" structure displayed greater resistance variations in the whole pressure range considered, showing that 3D structures with voids, not achievable without 3D printing, are more sensitive to pressure loads. Similarly to tensile trials, repeatability of "stars" sample under compression loads was assessed through cyclic compression electromechanical tests. Interestingly, it showed little variations between loading and unloading curves under 25 cycles of compression (figure S7a). This outcome is optimal for the reproducibility of sensor response under external repeated loads. Cycles of resistance variations are basically identical, indeed (figure S7b). Moreover, the sample shows also a fast response to the applied strain, with 0.53 s of response time and 0.76 s of recovery time (figure S8), fundamental properties for sensing applications.

Versatility is the key factor of this organohydrogel, as it possesses different types of stimulus sensitivity, an optimal durability, excellent strain and pressure lower detection limits and 3D printability, as reported in the literature comparison shown in Table 1. To validate these properties, the organohydrogel was tested as various types of wearable sensors. Initially, PVA/AAc/NaCl organohydrogel strip samples were applied to different parts of human body in order to prove their capability in bio-signals monitoring. The sensor was fixed through polyimide tape. It was applied to the index finger and it was bent at different velocities to demonstrate joint motion recognition (Fig. 5a). Organohydrogel sensor was effectively able to follow these deformations through resistance changes, returning to the initial resistance value when no strain was applied. The ability to sense tiny deformations was then proved. Swallowing as well as smaller strains associated to vocal chord vibration during words pronunciation were detected by the sensor applied on the volunteer's throat (Fig. 5b). Moreover, in Fig. 5c the resistance changes related to the deformation of the flexor muscle that control fingers movement, placed on the forearm, are reported. Fingers were bent to form a fist, and the hand was kept in this position for different durations. The optimal sensitivity of PVA/AAc/NaCl organohydrogel sensor to a wide variety of deformations suggests that other mechanical bio-signals could be detected in the same way.

To verify the applicability as temperature sensor, it was placed on a glass laboratory beaker, filled with water at different temperatures, through polyimide tape (Fig. 5d). The organohydrogels sensor adhered well to the bended surface of the beaker thanks to its optimal flexibility (inset of Fig. 5d). Electrical capacitance and resistance were measured through LCR meter and their dependency with respect to the temperature variation was derived. Sensor temperature was measured through a thermal camera (FLIR E6 Ex-Series) and capacitance and resistance were recorded at different temperature steps, starting from 5 °C. The initial

Table 1
Literature comparison for organohydrogels used as wearable sensors. Gauge factor in the strain range (0 %−55 %) mainly involved in human related movements is reported (NA = not available data, ***X*** = not tested, ✔= tested).

Material	Elongation at break	GF (0 %−55 % strain)	Durability	Lower detection limits	3D printable	Temperature sensing ($T > 0$ °C)	Humidity sensing	Ref
PVA/AAc/PEGDA/NaCl in DIW:Gly	350 %	0.85	180 days	0.05 % tensile strain, 1.5 Pa pressure	✔	✔ 5.61 % °C^{-1}	✔ 1.27 %/RH (%)	This work
PVA/CA/$CaCl_2$/Mxene in DIW:EG	388.3 %	0.771	15 days	2 % tensile strain	X	X	X	[76]
PVA/AAc/tannin/$AlCl_3$ in DIW:EG	850 %	~2	~ 4.2 days	1 % tensile strain	X	✔ NA	X	[7]
Goatskin collagen/Aam/TA/Ag NPs in DIW:EG	542 %	~2.4 ÷2.5	15 days	NA	X	✔ NA	✔ NA	[77]
Sheepskin/HPA/$AlCl_3$ in DIW:Gly	304.8 %	1.12	7 days	NA	X	✔ NA	X	[78]
PAM/Gelatin/LiCl in DIW:Gly	567 %	1.26	7 days	5 % tensile strain	X	✔ 5.72 % °C^{-1}	X	[65]
PVA/CNFs/$AlCl_3$ in DIW:DMSO	300 %	0.96	30 days	1 % tensile strain, 1 kPa pressure	X	✔ 4.66 % °C^{-1}	X	[79]
Silk fibroin /AAm/AAc/PEGDA/$MgCl_2$ in DIW:Gly	Up to 1200 %	1.29	10 days	NA	✔	X	X	[40]
Alginate/Gelatin/Multivalent Cation in DIW:Gly	Up to 140 %	1.67 ÷ 2.27	NA	NA	X	✔ 19 %C^{-1}	✔ 2.2 %/RH (%)	[80]
Agar or gellan gum or κ-carragenaan + NaCl in DIW:Gly	Up to 230 %	0.57	30 days	5 % tensile strain	X	✔ 2.1 %C^{-1}	✔ 1 %/RH(%)	[81]
CNF/PAM/Mxene in DIW:Gly	559 %	0.77	7 days	1 % tensile strain	X	X	X	[82]
AAm/AAc/Lauryl methacrylate/ hydroxyethyl cellulose/NaCl in DIW:Gly	Up to 1300 %	2.28	7 days	1 % tensile strain	✔	X	X	[70]

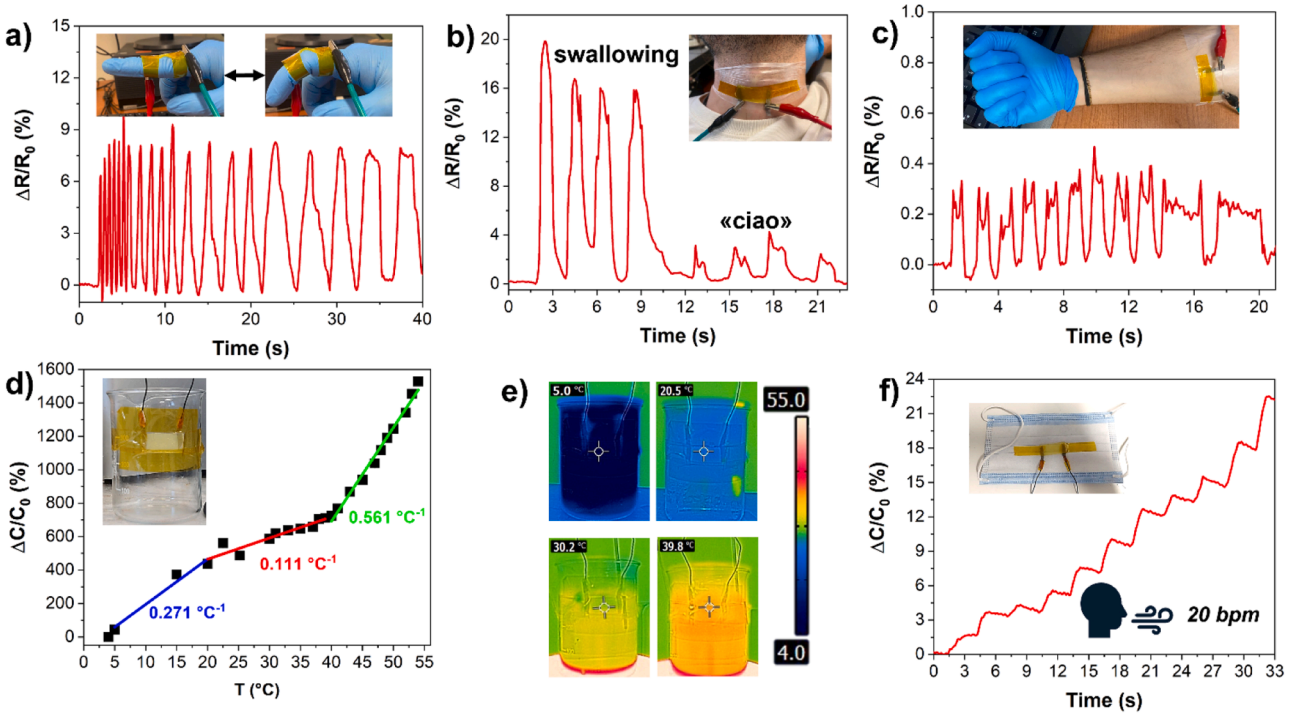

Fig. 5. . Organohydrogel resistance response under different deformation stimuli: finger bending (a), swallowing and vocal chords vibration during speech (b) and fingers muscle motion when fist is held for different durations (c). In the insets, the setups are shown. (d) Organohydrogel capacitance response to temperature variations. The raw data can be fitted in 3 linear regions, highlighted by the blue line (R^2=0.967), red line (R^2=0.888) and green line (R^2=0.986). In the inset, the sensor applied to the curved surface of a beaker is displayed. (e) Different sensor surface temperatures monitored by a thermal camera. (f) Organohydrogel resistance response to human breathing after a mild physical exercise. In the inset, the sensor applied on a mask is displayed. The breath per minute (bpm) recorded are reported too.

temperature was achieved by ice cubes addition to the beaker and then it was increased by placing the beaker on a hot plate (Fig. 5e, inset). The increase in capacitance with rising temperature is also linked to the enhanced ion mobility at higher temperatures. As temperature rises, charge transport and ion adsorption at the electrode interfaces improve, further enhancing the electrical double layer and leading to a higher capacitance value [44,83–85]. Capacitance transfer curve could be linearly approximated in three different regions, with a sensitivity of 0.271

$°C^{-1}$ between 4 °C and 20 °C, 0.111 $°C^{-1}$, between 20 °C and 40 °C and 0.561 $°C^{-1}$ between 40 and 55 °C respectively (Fig. 5e). These variations are greater than those observed in the resistance response (figure S9). In that case the resistance drops due to the softening of the polymeric matrix and enhanced ion mobility that therefore cause an increase of ionic conductivity as already described by DMTA analysis. This proof-of-concept experiment could for example simulate the potential to detect fever conditions, exploiting the temperature sensitivity of PVA/AAc/NaCl organohydrogel. Since its good sensitivity to both temperature and humidity stimuli, the organohydrogel sensor was fixed in the inner part of a commercial mask to monitor human breathing after a mild physical activity (Fig. 5d). Capacitance variations revealed an increasing trend due to the rise in both temperature and humidity in the closed space around the sensor, caused by the exhaled air from the lungs. However, the clearly visible cyclic peaks in capacitance represent the sudden increase in both temperature and humidity related to the respiratory activities. The number of breaths per minute could be derived by counting these peaks. It turned out to be about 20 bpm, in line with the respiratory rate of an adult person. This example demonstrates the potential for contactless monitoring of human breath. As shown in these examples, the excellent repeatability of response to both tensile and compressive stimuli, the sensibility to both micro and macro deformations and the temperature responsiveness, justify the potential employment of PVA/AAc/NaCl organohydrogel as wearable flexible sensor in a broad spectrum of applications.

4. Conclusion

Here a long-term durable organohydrogel for multi-stimuli flexible sensors is investigated. Water replacement strategy was adopted for a previous developed ionically conductive 3D printable hydrogel to address water evaporation issue. In particular, the PVA/AAc/NaCl hydrogel water was partially substitute with glycerol, a biocompatible and high boiling point solvent, by simply immersion. The so-called organohydrogel samples exhibited ionic conductivity and external deformations sensitivity through a piezoresistive transduction mode. A broad range of strains, starting from 0.05 % and up to 350 %, at various frequencies of deformation, could be monitored. The reduced water evaporation of this organohydrogel allows an outstanding stability up to 180 days and temperature sensing. Moreover, the -OH rich environment, provided by glycerol presence, enables the detection of humidity variations, exploiting both resistance and capacitance changes. Since the solvent replacement strategy is applied after the hydrogel samples curing, 3D printing advantages were maintained for the organohydrogel too. 3D printed “stars” structures was proven to exhibit an improved sensitivity to pressures with respect to a classic shape (“bulk”), with an exceptional limit of pressures detection of 1.5 Pa. The ability to monitor several human biosignals, like vocal chords vibration, breathing and temperature demonstrates the great versatility of PVA/AAc/NaCl organohydrogel, which potentially could be employed in wearables, soft robotics, HMI, where long-term stable sensors are necessary.

CRediT authorship contribution statement

Giorgio Mogli: Writing – review & editing, Writing – original draft, Investigation, Formal analysis, Conceptualization. **Ignazio Roppolo:** Writing – review & editing, Writing – original draft, Validation, Methodology, Data curation, Conceptualization. **Annalisa Chiappone:** Writing – review & editing, Validation, Resources, Methodology, Conceptualization. **Stefano Stassi:** Writing – review & editing, Validation, Supervision, Resources, Formal analysis, Data curation, Conceptualization.

Declaration of competing interest

The authors declare that they have no known competing financial interests or personal relationships that could have appeared to influence the work reported in this paper.

Acknowledgements

This research was supported by the Ministero dell’Università e della Ricerca (MUR), through PRIN 2022 - PASSO Prot.20222TKNRJ grant and the National Plan for Complementary Investments to the NRRP, project “D3-4Health - Digital Driven Diagnostics, prognostics and therapeutics for sustainable Health care” (project code:PNC0000001).

Supplementary materials

Supplementary material associated with this article can be found, in the online version, at doi:10.1016/j.apmt.2025.102675.

Data availability

Data will be made available on request.

References

[1] M. Zhu, T. He, C. Lee, Technologies toward next generation human machine interfaces: from machine learning enhanced tactile sensing to neuromorphic sensory systems, Appl. Phys. Rev. 7 (3) (2020).
[2] Y. Yang, W. Gao, Wearable and flexible electronics for continuous molecular monitoring, Chem. Soc. Rev. 48 (6) (Mar 18 2019) 1465–1491, https://doi.org/10.1039/C7CS00730B.
[3] T. Sun, et al., Artificial intelligence meets flexible sensors: emerging smart flexible sensing systems driven by machine learning and Artificial synapses, Nanomicro Lett. 16 (1) (Nov 13 2023) 14.
[4] S. Pyo, J. Lee, K. Bae, S. Sim, J. Kim, Recent progress in flexible tactile sensors for Human-interactive systems: from sensors to advanced applications, Adv. Mater. 33 (47) (Nov 2021) e2005902.
[5] Z. Zhang, F. Xiang, D. Mei, Y. Wang, Waterproof and flexible aquatic tactile sensor with interlocked ripple structures for broad range force sensing, Adv. Mater. Technol. 9 (2) (2023) 2301513, 2024/01/01.
[6] Y. Mi, Z. Zhao, Y. Lu, X. Cao, N. Wang, Mussel-inspired ionic hydrogel for tactile perception: toward versatility, robustness and sustainability, Chem. Eng. J. 491 (2024) 151770, 2024/07/01/.
[7] B. Song, X. Dai, X. Fan, H. Gu, Wearable multifunctional organohydrogel-based electronic skin for sign language recognition under complex environments, J. Mater. Sci. Technol. 181 (2024) 91–103, 2024/05/10/.
[8] M.T.N. Nguyen, T.D. Nguyen, J.H. Han, J.S. Lee, Synthesis of PDMS chain structure with introduced dynamic covalent bonding for high-performance rehealable tactile sensor application, Small. Methods 8 (12) (Dec 2024) e2400163.
[9] W. Suh, et al., Small-sized deformable shear sensor array for direct monitoring of quantitative shear distribution, Adv. Mater. Technol. 7 (6) (2021) 2101071.
[10] H. Li, et al., Piezoresistive-piezocapacitive hybrid pressure sensor based on synergetic MXene porous conducting and ion trapping effects for operando battery state-of-charge monitoring, Chem. Eng. J. 497 (2024) 154929, 2024/10/01/.
[11] N. Wang, et al., Tactile sensor from self-chargeable piezoelectric supercapacitor, Nano Energy 56 (2019) 868–874, 2019/02/01/.
[12] J. Seong, B.-U. Bak, D. Lee, J. Jin, J. Kim, Tribo-piezoelectric synergistic BaTiO3/PDMS micropyramidal structure for high-performance energy harvester and high-sensitivity tactile sensing, Nano Energy 122 (2024) 109264, 2024/04/01/.
[13] H. Zhu, J. Liang, J. Huang, Z. Chen, Triboelectric haptic sensors based on fluorinated cellulose/PDMS composite porous films for monitoring joint flexion and smart writing, Nano Energy 127 (2024) 109735, 2024/08/01/.
[14] H. Yang, et al., A novel triboelectric-optical hybrid tactile sensor for human-machine tactile interaction, Nano Energy 125 (2024) 109592. /06/15/2024.
[15] J. Shen, Y. Yang, J. Zhang, W. Lin, H. Gu, Carbon quantum dot-functionalized Dermis-derived transparent electronic skin for multimodal Human motion signal monitoring and construction of self-powered triboelectric nanogenerator, ACS. Appl. Mater. Interfaces. 16 (35) (Sep 4 2024) 46771–46788.
[16] X. Xiong, et al., Polymerizable rotaxane hydrogels for three-dimensional printing fabrication of wearable sensors, Nat. Commun. 14 (1) (Mar 10 2023) 1331.
[17] C. Ma, et al., Highly processable ionogels with mechanical robustness, Adv. Funct. Mater. 33 (31) (2023).
[18] A. Chiappone, I. Roppolo, E. Scavino, G. Mogli, C.F. Pirri, S. Stassi, Three-dimensional printing of triboelectric nanogenerators by digital light processing technique for mechanical energy harvesting, ACS. Appl. Mater. Interfaces. 15 (46) (Nov 22 2023) 53974–53983.
[19] C. Zhang, et al., 3D Printed, solid-State conductive ionoelastomer as a generic building block for tactile applications, Adv. Mater. 34 (2) (Jan 2022) e2105996.
[20] B. Payandehjoo, T.H. Kwok, Embedding ionic hydrogel in 3D printed human-centric devices for mechanical sensing, J. Manuf. Process. 100 (2023) 1–10.

[21] X. Yue, C. Fang, Q. Yao, C. Liu, C. Shen, H. Liu, Tunable porous fiber-shaped strain sensor with synergistic conductive network for human motion recognition and tactile sensing, Chem. Eng. J. 491 (2024) 151853, 2024/07/01/.
[22] M. Zhang, et al., Biomimetic electronic skin through hierarchical polymer structural design, Adv. Sci. (Weinh) 11 (7) (Feb 2024) e2309006.
[23] D.J. Lipomi, et al., Skin-like pressure and strain sensors based on transparent elastic films of carbon nanotubes, Nat. Nanotechnol. 6 (12) (Oct 23 2011) 788–792.
[24] A.P. Gerratt, H.O. Michaud, S.P. Lacour, Elastomeric electronic skin for prosthetic tactile sensation, Adv. Funct. Mater. 25 (15) (2015) 2287–2295, 2015/04/01.
[25] X. Guo, et al., Human touch sensation-inspired, ultrawide-sensing-range, and high-robustness flexible piezoresistive sensor based on CB/MXene/SR/fiber nanocomposites for wearable electronics, Compos. Struct. 321 (2023) 117329. /10/01/2023.
[26] K. Pang, et al., Hydroplastic foaming of graphene aerogels and artificially intelligent tactile sensors, Sci. Adv. 6 (46) (Nov 2020) eabd4045.
[27] Y.S. Zhang, A. Khademhosseini, Advances in engineering hydrogels, Science (1979) 356 (6337) (May 5 2017,).
[28] L. Wang, T. Xu, X. Zhang, Multifunctional conductive hydrogel-based flexible wearable sensors, TrAC, Trends Anal. Chem. 134 (2021) 116130, 2021/01/01/.
[29] M. Caprioli, I. Roppolo, A. Chiappone, L. Larush, C.F. Pirri, S. Magdassi, 3D-printed self-healing hydrogels via Digital Light processing, Nat. Commun. 12 (1) (Apr 28 2021) 2462.
[30] Q. Zhou, et al., Mechanically strong and multifunctional hybrid hydrogels with ultrahigh electrical conductivity, Adv. Funct. Mater. 31 (40) (2021) 2104536.
[31] J. Chen, et al., Multifunctional conductive Hydrogel/Thermochromic elastomer hybrid fibers with a core-shell segmental configuration for wearable strain and temperature sensors, ACS. Appl. Mater. Interfaces. 12 (6) (Feb 12 2020) 7565–7574.
[32] P. Song, H. Qin, H.L. Gao, H.P. Cong, S.H. Yu, Self-healing and superstretchable conductors from hierarchical nanowire assemblies, Nat. Commun. 9 (1) (Jul 17 2018) 2786.
[33] B. Yao, et al., Ultrahigh-conductivity polymer hydrogels with arbitrary structures, Adv. Mater. 29 (28) (Jul 2017) 1700974.
[34] S. Zhang, et al., Room-temperature-formed PEDOT:PSS hydrogels enable injectable, soft, and healable organic bioelectronics, Adv. Mater. 32 (1) (Jan 2020) e1904752.
[35] J. Song, et al., Mechanically and electronically robust transparent organohydrogel fibers, Adv. Mater. 32 (8) (Feb 2020) e1906994.
[36] J. Zhang, et al., Mechanically robust, flexible, fast responding temperature sensor and high-resolution array with ionically conductive double cross-linked hydrogel, Adv. Funct. Mater. 34 (21) (2024) 2314433.
[37] L. Zhao, C. Fang, B. Qin, X. Yang, P. Poechmueller, Conductive dual-network hydrogel-based multifunctional triboelectric nanogenerator for temperature and pressure distribution sensing, Nano Energy 127 (2024) 109772. /08/01/2024.
[38] H. Zhang, et al., Intrinsically stretchable jellyfish-like gold nanowires film as multifunctional wearable chemical and physical sensors, Chem. Eng. J. 490 (2024) 151798, 2024/06/15/.
[39] L. Zou, et al., Strong and anti-freezing alginate-based hydrogel with humidity response and wide-temperature-range strain sensing ability, Polymer. (Guildf) 295 (2024) 126735, 2024/03/01/.
[40] K. Wu, et al., 3D Printed silk fibroin-based hydrogels with tunable adhesion and stretchability for wearable sensing, Adv. Funct. Mater. 34 (46) (2024) 2404451.
[41] H. Yan, et al., 3D printing of dual cross-linked hydrogel for fingerprint-like iontronic pressure sensor, Smart Mater. Struct. 31 (1) (2021).
[42] D. Buenger, F. Topuz, J. Groll, Hydrogels in sensing applications, Prog. Polym. Sci. 37 (12) (2012) 1678–1719, 2012/12/01/.
[43] Y. Long, et al., Super-stretchable, anti-freezing, anti-drying organogel ionic conductor for multi-mode flexible electronics, Adv. Funct. Mater. 33 (41) (2023) 2304625, 2023/10/01.
[44] G. Mogli, A. Chiappone, A. Sacco, C.F. Pirri, S. Stassi, Ultrasensitive piezoresistive and piezocapacitive cellulose-based ionic hydrogels for wearable multifunctional sensing, ACS. Appl. Electron. Mater. 5 (1) (2022) 205–215.
[45] Z. Li, et al., Gelatin methacryloyl-based tactile sensors for medical wearables, Adv. Funct. Mater. 30 (49) (Dec 1 2020).
[46] Z. Li, et al., Anti-freezing, recoverable and transparent conductive hydrogels co-reinforced by ethylene glycol as flexible sensors for human motion monitoring, Int. J. Biol. Macromol. 230 (Mar 1 2023) 123117.
[47] Z. Zhang, et al., Highly transparent, self-healable, and adhesive organogels for bio-inspired intelligent ionic skins, ACS. Appl. Mater. Interfaces. 12 (13) (Apr 1 2020) 15657–15666.
[48] X. Huang, C. Wang, L. Yang, X. Ao, Highly stretchable, self-adhesive, antidrying ionic conductive organohydrogels for strain sensors, Molecules. 28 (6) (Mar 21 2023).
[49] L. Han, et al., Mussel-inspired adhesive and conductive hydrogel with long-lasting moisture and extreme temperature tolerance (in English), Adv. Funct. Mater. 28 (3) (Jan 17 2017) 1704195.
[50] J.L. Dashnau, N.V. Nucci, K.A. Sharp, J.M. Vanderkooi, Hydrogen bonding and the cryoprotective properties of glycerol/water mixtures, J. Phys. Chem. B 110 (27) (Jul 13 2006) 13670–13677.
[51] Z. He, W. Yuan, Adhesive, stretchable, and transparent organohydrogels for antifreezing, antidrying, and sensitive ionic skins, ACS. Appl. Mater. Interfaces. 13 (1) (Jan 13 2021) 1474–1485.
[52] X. Pan, et al., Ultraflexible self-healing guar gum-glycerol hydrogel with injectable, antifreeze, and strain-sensitive properties, ACS. Biomater. Sci. Eng. 4 (9) (Sep 10 2018) 3397–3404.
[53] S. Shi, X. Peng, T. Liu, Y.-N. Chen, C. He, H. Wang, Facile preparation of hydrogen-bonded supramolecular polyvinyl alcohol-glycerol gels with excellent thermoplasticity and mechanical properties, Polymer. (Guildf) 111 (2017) 168–176, 2017/02/24/.
[54] H. Gao, et al., Adaptive and freeze-tolerant heteronetwork organohydrogels with enhanced mechanical stability over a wide temperature range, Nat. Commun. 8 (1) (Jun 22 2017) 15911.
[55] C. Li, X. Deng, X. Zhou, Synthesis antifreezing and antidehydration organohydrogels: one-step In-situ gelling versus two-step solvent displacement, Polymers. (Basel) 12 (11) (2020) 2670.
[56] J. Wu, et al., Ultrastretchable and stable strain sensors based on antifreezing and self-healing ionic organohydrogels for Human motion monitoring, ACS. Appl. Mater. Interfaces. 11 (9) (Mar 6 2019) 9405–9414.
[57] F. Chen, et al., Rational fabrication of anti-freezing, non-drying tough organohydrogels by one-pot solvent displacement, Angew. Chem. Int. Ed. Engl. 57 (22) (May 28 2018,) 6568–6571.
[58] J. Wu, et al., An intrinsically stretchable humidity sensor based on anti-drying, self-healing and transparent organohydrogels, Mater. Horiz. 6 (3) (2019) 595–603, https://doi.org/10.1039/C8MH01160E.
[59] C. Li, X. Deng, X. Zhou, Synthesis antifreezing and antidehydration organohydrogels: one-step In-situ gelling versus two-step solvent displacement, Polymers. (Basel) 12 (11) (Nov 12 2020) 2670.
[60] G. Mogli, et al., Self-powered integrated tactile sensing system based on ultrastretchable, Self-healing and 3D printable ionic conductive hydrogel, Adv. Funct. Mater. 34 (7) (2023).
[61] G. Mogli, A. Chiappone, I. Roppolo, S. Stassi, Highly stretchable, 3D printable ionically conductive organohydrogel for long-time stable strain sensors, in: 2024 IEEE International Conference on Flexible and Printable Sensors and Systems (FLEPS), 2024, pp. 1–4.
[62] A.R. Velez, J.R. Mufari, L.J. Rovetto, Sodium salts solubility in ternary glycerol+water+alcohol mixtures present in purification process of crude glycerol from the biodiesel industry, Fluid. Phase Equilib. 497 (2019) 55–63. Article.
[63] S. Sanwlani, P. Kumar, H.B. Bohidar, Hydration of gelatin molecules in glycerol-water solvent and phase diagram of gelatin organogels, J. Phys. Chem. B 115 (22) (Jun 9 2011) 7332–7340.
[64] L. Jiang, et al., Flexible wearable sensors based on lignin doped organohydrogels with multi-functionalities, Chem. Eng. J. 430 (2022) 132653. /02/15/2022.
[65] L. Xu, X. Li, J. Gao, M. Yan, Q. Wang, Environment-tolerant gelatin based ionic conductive organohydrogel for flexible sensor, Mater. Today Commun. 40 (2024) 109542. /08/01/2024.
[66] Y. Deng, et al., Self-recoverable and mechanical-reinforced hydrogel based on hydrophobic interaction with self-healable and conductive properties, Chem. Eng. J. 353 (2018) 900–910. /12/01/2018.
[67] H. An, et al., A self-healing, long-lasting adhesive, lignin-based polyvinyl alcohol organo-hydrogel for strain-sensing applications, Int. J. Biol. Macromol. 279 (Nov 2024) 135509. Pt 4.
[68] S. Zhou, Z. Zhang, W. Zhong, A. Meng, Y. Su, Polyvinyl alcohol/PEDOT:PSS with Fe(3+)/amylopectin enabled highly tough, anti-freezing and healable hydrogels for multifunctional wearable sensors, Talanta 279 (Nov 1 2024) 126592.
[69] D. Hardman, J. Hughes, T.G. Thuruthel, K. Gilday, F. Iida, 3D Printable sensorized soft gelatin hydrogel for multi-material soft structures, IEEE Robot. Autom. Lett. 6 (3) (2021) 5269–5275.
[70] Z. Guo, H. Zhang, W. Xie, A. Tang, W. Liu, 3D printing hydrogel with structural design via vat photopolymerization for strain sensing, Addit. Manuf. 77 (2023) 103824, 2023/09/05/.
[71] T. Yamada, et al., A stretchable carbon nanotube strain sensor for human-motion detection, Nat. Nanotechnol. 6 (5) (May 2011) 296–301.
[72] S. Stassi, V. Cauda, G. Canavese, C.F. Pirri, Flexible tactile sensing based on piezoresistive composites: a review, Sensors. (Basel) 14 (3) (Mar 14 2014) 5296–5332.
[73] X. Hu, J. Zhou, W.F.M. Daniel, M. Vatankhah-Varnoosfaderani, A.V. Dobrynin, S. S. Sheiko, Dynamics of dual networks: strain rate and temperature effects in hydrogels with reversible H-bonds, Macromolecules. 50 (2) (2017) 652–659, 2017/01/24.
[74] Y. Tang, Z. Yu, L.-h. Tam, A. Zhou, D.M. Li, Behaviors of water molecules in polyvinyl alcohol gel amid stretch and temperature changes: a molecular dynamics study, Mater. Today Commun. 33 (2022) 104834. /12/01/2022.
[75] Z. He, J. Shen, M. Lan, H. Gu, Collagen fiber-reinforced, tough and adaptive conductive organohydrogel e-skin for multimodal sensing applications, J. Mater. Chem. B 12 (28) (Jul 17 2024) 6940–6958.
[76] X. Liu, et al., Highly conductive and stable double network carrageenan organohydrogels for advanced strain sensing and signal recognition arrays, Int. J. Biol. Macromol. 279 (Nov 2024) 135029. Pt 1.
[77] R. Zhao, et al., Ultra-flexible, anti-freezing, and adhesive collagen Fiber-derived conductive organohydrogel E-skin for strain, humidity, temperature, and bioelectric sensing applications, Chem. Mater. 36 (17) (2024) 8141–8158, 2024/09/10.
[78] Y. Yang, B. Song, J. Zhang, N. Dan, H. Gu, Multifunctional, high-strength electronic skin based on the natural sheepskin Fiber network for multifaceted Human health monitoring and management, Biomacromolecules. 25 (8) (Aug 12 2024) 5359–5373.
[79] M. Li, et al., An environmentally tolerant, highly stable, cellulose nanofiber-reinforced, conductive hydrogel multifunctional sensor, Carbohydr. Polym. 284 (2022) 119199. May 15,.

[80] P. Tordi, A. Tamayo, Y. Jeong, M. Bonini, P. Samorì, Multiresponsive ionic conductive alginate/gelatin organohydrogels with tunable functions, Adv. Funct. Mater. 34 (52) (2024) 2410663.
[81] L. Ye, R. Yang, X. Yu, X. Sun, H. Liang, Strong and tough polysaccharide organohydrogels for strain, humidity and temperature sensors, Soft. Matter. 20 (7) (Feb 14 2024) 1573–1582, https://doi.org/10.1039/D3SM01281F.
[82] W. Zhang, et al., Stretchable, antifreezing, non-drying, and fast-response sensors based on cellulose nanocomposite hydrogels for signal detection, Macromol. Mater. Eng. 306 (12) (2021) 2100549.
[83] Y. Yu, S. Peng, M. Islam, S. Wu, C.H. Wang, Wearable supercapacitive temperature sensors with high accuracy based on ionically conductive organogel and macro-kirigami electrode, Adv. Mater. Technol. 8 (4) (2023) 2201020.
[84] Z. Wu, et al., Ultrasensitive, stretchable, and fast-response temperature sensors based on hydrogel films for wearable applications, ACS. Appl. Mater. Interfaces. 13 (18) (2021) 21854–21864, 2021/05/12.
[85] H. Ota, et al., Highly deformable liquid-state heterojunction sensors, Nat. Commun. 5 (1) (2014) 5032, 2014/09/29.